

Cluster and statistical analysis of spatial earthquake patterns in the South Caucasus region

Sergii Skurativskyi^{1,1}, Sergiy Mykulyak¹, Yuliya Semenova^{1,2}, Kateryna Skurativska³

¹ S.I.Subbotin Institute of Geophysics of the National Academy of Science of Ukraine,
Kyiv, Ukraine

² DGFI-TUM, Technical University of Munich, Munich, Germany

³ University of Padova, Padova, Italy

Abstract. The Caucasus region is characterized by heterogeneous and strong seismicity as a result of collision between Arabian and Eurasian tectonic plates. A rich variety of seismic events also distinguishes Azerbaijan, located in its south part. In this research, we consider the earthquakes, specifically spatial earthquake patterns that occurred in Azerbaijan and adjacent areas from 2010 to 2023. Applying density-based clustering algorithms to the earthquake catalog, the proper partitions of spatial earthquake distributions were obtained. The statistical properties of the catalog's partition into 7 clusters are studied in more detail. In particular, we consider the random variable, which is the distance from the fixed point of the earth's surface to earthquake epicenters. The analytical approximation of the cumulative distribution function is constructed for the case when the fixed point coincides with the cluster center and epicenters in the cluster are distributed by the bivariate normal distribution. For comparison, the numerical distribution functions are evaluated on the basis of Johnson curves and good agreement is observed. Another case is also considered when the fixed point lies outside of a cluster. Under the assumption that a cluster is a circle and epicenters in it are distributed uniformly, the cumulative and probability distribution functions are derived. Applying these functions to the approximation of histograms for the distances from the Shamkir hydroelectric power station to the clusters shows that satisfactory agreement can be achieved. These results are promising for performing the seismic risk assessment for the Shamkir station or other objects of Azerbaijan's critical infrastructure.

Keyword: Spatial earthquake distribution, Earthquake clustering, Density-based spatial clustering, Seismicity of Caucasus region.

Introduction

1 Introduction

As is known from [1], between 50 and 80 earthquakes are registered daily on the Earth. Although a significant portion of them are quite weak and do not pose a significant threat, a few thousand earthquakes each year are still extremely destructive and dangerous. Typically,

¹e-mail: skurserg@gmail.com

such strong earthquakes occur near seismic belts, in areas of oceanic ridges, and continental rift zones.

This fully applies to the Caucasus region, where the Greater Caucasus mountain belt is located together with fold-and-thrust belts and a series of depressions [2–6]. Particularly, the South Caucasus, covering the territories of Azerbaijan, Armenia, and Iran, corresponds to the intercontinental collision zone [3] and is represented by the Kura, Baiburt-Garabagh-Kaphan and Talysh foreland fold-and-thrust belts [6]. These zones are seismically active zones connected to the rapid and non-uniform plate convergence between Arabia and Eurasia and exhibit thin-skinned tectonics with fault-bend folds, fault-propagation folds, and duplexes [2]. Among the manifestations of active tectonics of the region, we are interested in the set of earthquakes, the properties of which are important for developing models of seismic activity, mechanisms of earthquakes, and forecasting [5, 7], as well as for the effective conduct of economic or other activities, reducing the level of seismic danger, etc.

Since this is a densely populated region, rich in mineral resources (gas, oil, etc.), the study of the Caucasus seismicity and the implementation of earthquake-safe technologies are the subject of many studies [2–5], however, with the development of a seismic station network, by improving the methods of collecting, processing and exchanging seismic data, by developing mathematical and informational methods of data research, such investigations are constantly being deepened and supplemented.

Thus, issues related to identifying groups of earthquakes, i.e. clustering, gained a new impetus for development. The understanding of clustering as a set of aftershocks triggered by the main event was expanded by the interpretation of clustering as the processing of abstract events with the aim of identifying similar features using special cluster analysis algorithms [8].

In particular, this research extends previous investigations of [9, 10] related to the analysis of seismic safety of the territories of Azerbaijan. In studies by [9, 10], attention was drawn to the research of the Shamkir-Mingachevir reservoir region, where two hydroelectric power stations (HPSs) are located. Using ground response analysis, local site effects in the vicinity of HPSs were analyzed and recommendations for taking such effects into account were proposed.

This study examines the seismicity of Azerbaijan and surrounding areas and discusses the impact of South Caucasus seismicity on local facilities such as the Shamkir HPS. In particular, using modern approaches in statistical seismology and clustering algorithms, a subset of earthquake epicenters is grouped into *spatial* clusters [8, 11, 12], which help to define the shapes of seismogenic zones. The cumulative distribution functions (CDFs) and probability density functions (PDFs) for the distances from a fixed point on the earth’s surface to cluster points are constructed. Cases where the distribution functions allow for analytical research are considered, and numerical approximations of the distribution functions are also proposed. Specifically, by utilizing the relevant distribution functions, the connection of clusters with the Shamkir HPS is analyzed to develop the theoretical foundations of seismic risk assessment.

2 The earthquakes in South Caucasian and their clustering

We consider the South Caucasus region the rectangle enclosed by the Latitude range 38° to 42° N and the Longitude range 45° to 50° E incorporating Azerbaijan.

Using the databases of the International Seismological Centre [13], the catalog of earthquakes occurred from 01.01.2010 to 31.12.2023. The catalog is quite uneven by year; for instance, there are about 1200 entries for the years 2010-2013 and about 800 entries for 2014-2017, whereas for 2018-2023, there are already about 4000 entries. In this research, as in [5], we consider earthquakes with magnitude equal to or larger than 2 ($M \geq 2$). Depending on the objectives of the study, the lower threshold magnitude can be specified in different ways. One of them is based on the evaluation of the completeness magnitude M_c providing the seismic catalog completeness. To get a rough estimate for M_c , the MAXC method [5,12] can be used. As shown in Appendix C, we can use a rough estimate $M_c = 2$ and further consider all earthquakes with $M \geq M_c$.

Next, we are going to deal only with the epicenter coordinates, although certain stages of research can be performed for a more complete list of earthquake characteristics (depth, magnitude, etc.). The resulting dataset on the locations of earthquake epicenters from the specified rectangle contains 6097 entries. This dataset is subjected to the clustering procedure, which applies the appropriate clustering algorithms. An overview of this is given in the next section.

2.1 Survey of clustering algorithms and their application to analysis of seismicity

Currently, cluster analysis as a tool for the automatic analysis of data of different natures is rapidly developing. Evidence of this is the development of more than a dozen data clustering methods, and the number of clustering algorithms alone already exceeds a hundred.

The most well-known and widely implemented methods include Partitioning Methods (k-means and its modifications k-medians, k-medoids), Density-Based Methods (DBScan and its modifications HDBScan, OPTICS, ST - DBSCAN - EV [14]), Hierarchical Methods (Agglomerative, Divisive), Grid-Based Methods (STING, CLIQUE) and many others [15]. The use of clustering algorithms is designed to reduce the influence of the human factor in data analysis and to automate the same type of work, but the most important thing is to try to identify new regularities and properties in datasets that are difficult to formalize and can be described in fuzzy logic [16].

Therefore, the application of these algorithms to earthquake sequences is more than justified and, as evidenced by the analysis of literary sources, exhibits steady progress. In particular, in the work by [17], clustering analysis is applied to moment tensor catalogs, including mining-induced microseismic data. The proposed approach also made it possible to classify earthquake point source models and detect and characterize clusters of focal mechanisms, which potentially allows for the assessment of time-varying hazards in mines. The problems of induced seismicity were also considered in the paper by [18] when the maximum magnitude earthquake is evaluated caused by the operation of an injection well in Colorado. The developed method incorporates the DBSCAN algorithm for classifying individual clusters and assessing the geometry of individual seismicity clusters. A comparison

of the performance of K-means and DBSCAN algorithms with a set of worldwide seismic events that occurred from 1965 to 2016 was carried out by [19]. The quality of clustering was evaluated based on the comparison of the obtained clusters with known seismic belts. As a result of the research, it was concluded that the DBSCAN algorithm has a significant advantage when working with earthquakes.

[20] describes the experience of applying the DBSCAN and OPTICS algorithms to analyze earthquake catalogs of 2016 Kumamoto and 2016 Central Italy sequences. The authors carried out extensive analysis concerning the influence of the algorithm parameters on clustering results during explorations of earthquake catalogs. They also concluded that the graphical representation of the spatial distribution of hypocenters and their density helps select the algorithm parameters. Although the selection of input parameters and the type should be made carefully, cluster solutions can provide helpful information about the characteristic structures of a dataset, features of seismic sequences, and the scenarios of the spatiotemporal evolution of fault systems.

Clustering of earthquakes in the region of the Alto Tiberina Fault system (Central Italy) was also used in the studies of [21], in which a correlation between clustering and earthquake size distributions was revealed that allows one to assess relations of background and triggered seismicity.

The studies of [16] are devoted to identifying seismotectonic provinces in the Iranian Plateau using the fuzzy clustering algorithm. In particular, the spatial distributions of earthquake epicenters were partitioned, and the clustering results were compared with the active faults and seismotectonic models.

Similar problems of detecting the clusters of aftershocks and independent background seismic events were considered in the paper by [22], where a two-stage clustering approach based on a density-based clustering algorithm was developed. Special attention is paid to analyzing the space-time clustering of an earthquake catalog, including the epicenter plot for California, the Himalayas, Japan, and Sumatra–Andaman.

Using the original ST-DBSCAN-EV algorithm, the authors of [14] applied cluster analysis to the three large earthquakes in Chile. They identified the precursor seismic activity, the emergence of seismic swarms, and periods of foreshocks and aftershocks.

Recent studies of [23] dealt with the spatial clustering of seismic events forming the Petrinja (Croatia) earthquake sequence. Using the DBSCAN algorithm, several clusters were identified, and their statistical properties in terms of the Tsallis entropy technique were considered.

Due to the rapid development of machine learning tools and clustering methods, in particular, it is obvious that it is not possible to cover all the current publications in this field of research, even the most significant ones. Therefore, we will conclude the literature review with a few of the most recent works. The (H)DBSCAN algorithms were used in [24] for geospatial and temporal analysis of seismicity near Mt. Ruapehu, New Zealand, including the identification of earthquake swarms that occurred in the region. The main feature of this research is the experience of applying cluster analysis combined with a comprehensive interpretation of the results that provides a deeper understanding of the processes in seismically active zones. A similar issue related to an earthquake swarm in Italy was considered in [25] where the unique approach for automatically processing clusters of seismicity was developed. The seismicity of Central Italy 2016–2017 was studied in [26] with the help of the fully automatic algorithm designed within the framework of the HDBSCAN, DBSCAN,

SOM and OPTICS cluster algorithms. Using the clustering technique and neural network, a methodology for detecting tectonic tremors among fast earthquakes and anthropogenic events was developed in [27]. To revise the seismic catalog of mainland France from 2010 to 2018, in [28], a new workflow was established utilizing the HDBSCAN algorithm. By applying the HDBSCAN algorithm and statistical methods, the basic elements of spatial clustering and survival analysis of the temporal and spatial patterns for earthquake data were demonstrated with Python code developed by [29].

Taking the recommendations into account, particularly those referred to in the references above, regarding the use of algorithms for clustering actual earthquakes [11, 30], it was decided to apply the DBSCAN and HDBSCAN algorithms in the research.

Let us briefly recall these algorithms' main features [11, 31, 32]. Since they belong to the density-based clustering algorithms, the partition of a dataset consists of subsets that differ in density. To evaluate the density near a sample point, we construct the hyper-sphere of radius ε (local ε -neighborhood) and predefine a minimal number of samples (*Min_sample*) to consider the set of points in the hyper-sphere as a cluster. This pair of intrinsic parameters ε and *Min_sample* governs the algorithm work [11]. All points of the dataset are qualified by core (its ε -neighborhood contains no less than *Min_sample* points including the point of observation), border (it is not the core point but its ε -neighborhood contains at least one core point), and noise points (it is neither a core point nor a border point). The separated cluster is constructed on the basis of two notions: the density-reachable pair of core points and the density-connected sequence of density-reachable points. The DBSCAN's main advantages are as follows: does not require pre-definition of a number of clusters; can identify the clusters of arbitrary shapes; uses only two understandable parameters, while its disadvantages [32] include: it is rather sensitive to the variations of ε [30] and *Min_sample*; may fail when working with the clusters of significantly varying densities; adding new points into the starting dataset requires restarting the algorithm. Other pros and cons can be found elsewhere [33]. HDBSCAN [32, 33] is an advanced version of DBSCAN performing the clustering over varying ε providing the identification of clusters with varying densities.

Apart from clustering algorithms, cluster analysis also covers other issues, including the estimation of a number of clusters and intrinsic parameters of algorithms, data preprocessing, dimension reduction for multidimensional data, and cluster validation related to assessment of the clustering quality [15].

In particular, cluster validation means estimating how well the proposed partition fits the input data and is based on considering the specific measure-validity indices. Various indices stimulate their intensive comparative treatment [34–36]. Here we used the Silhouette index (or Silhouette score) (*Slh*) proposed by [37]. This index is commonly used in cluster analysis [38, 39], including earthquake catalogs [24, 40], and exhibits acceptable computational complexity and clear interpretation. Let us provide a short description of *Slh*.

When the set C is partitioned by N clusters C_i , $i = 1, \dots, N$, then for each cluster C_i the Silhouette index is evaluated as follows

$$Slh(C_i) = \frac{1}{|C_i|} \sum_{j=1}^{|C_i|} s(j), \quad (1)$$

where $|C_i|$ is the number of elements in the C_i cluster and

$$s(i) = \frac{a(i) - b(i)}{\max\{a(i), b(i)\}}$$

is the sample Silhouette score. The mean intra-cluster distance $a(i)$ and mean nearest-cluster distance $b(i)$ are calculated by means of the following relations

$$a(i) = \frac{1}{|C_i| - 1} \sum_{j=1}^{|C_i|} d(i, j), \quad b(i) = \min_{k \neq i} \sum_{j=1}^{|C_k|} d(i, j)$$

where $d(i, j)$ is a distance (euclidean or cityblock).

By analogy, the Silhouette score for the set C is the mean value for all $s(i)$, i.e $Slh(C) = \sum_{i=1}^N s(i)/N$.

When all clusters are well separated and dense enough, $Slh(C)$ is close to 1. The low positive $Slh(C)$ value indicates poorly separated clusters. When $-1 < Slh(C) < 0$, the elements refer to misclassified. Note that the Slh technique works well when clusters are well localized and convex. Moreover, they should be linearly separable. When clusters possess complex shapes and mutual locations do not allow one to separate them by straight lines, then Slh can provide incorrect estimates. Such a situation occurs, for instance, when DBSCAN algorithms are used, in which clusters are determined by the density of points and can have any geometry. Therefore, a high Slh , more than 0.5-0.7, is accepted, which means a confident partition into clusters. A small or negative Slh does not always mean a lousy partition and may require a more detailed analysis of clusters.

2.2 Clustering of Earthquake Catalog using DBSCAN algorithm

To carry out the clustering procedure, we use application packages developed with Python 3.11, specifically the module *sklearn.cluster* elaborated within the scikit-learn (ver.1.6) project [41]. Python source code implementing the DBSCAN and HDBSCAN (as well as K-means for comparison) algorithms and calculation of Silhouette, Calinski-Harabasz (CH), Davies-Bouldin (DB) indices is available at https://github.com/SkurativskaKateryna/AGPH_Earthquake_Clustering_Analysis.git.

There is no generally accepted methodology to date for estimating parameters for the DBSCAN algorithm [11, 20, 31]. Therefore, we apply a kind of the grid search technique to optimize the partition using the DBSCAN algorithm, which involves testing various discrete combinations of key parameters to identify the best-performing configuration based on the Silhouette score. The preliminary estimation for ε is obtained by applying the procedure based on the sorted k -distance graph. This procedure, described in detail in Appendix D, was implemented taking into account the recommendations of [31].

Based on this, we explored a discrete parameter space spanned by the sets: $\varepsilon \in [0.2, 1.0]$ with a step of 0.1; $Min_samples \in [25; 350]$ with a step of 25; and $metric \in \{euclidean, manhattan\}$. This range was selected to encourage the formation of 5 to 10 meaningful clusters, as cases producing fewer than 2 clusters or more than about 20 clusters were deemed either uninformative or excessively fragmented. From the total parameter combinations, 113 valid clusterings (with at least two clusters) were retained. For each partition, the Silhouette score was computed to assess clustering quality (Fig. 1a), with similar trends observed when varying either ε or $Min_samples$. Ultimately, we can conclude that large values of both parameters generally produced fewer clusters, no more than 5.

Instead, let us consider the partitions with 6 to 8 clusters, which may be better suited to territories with an extremely dense fault network. The most features of such partitions

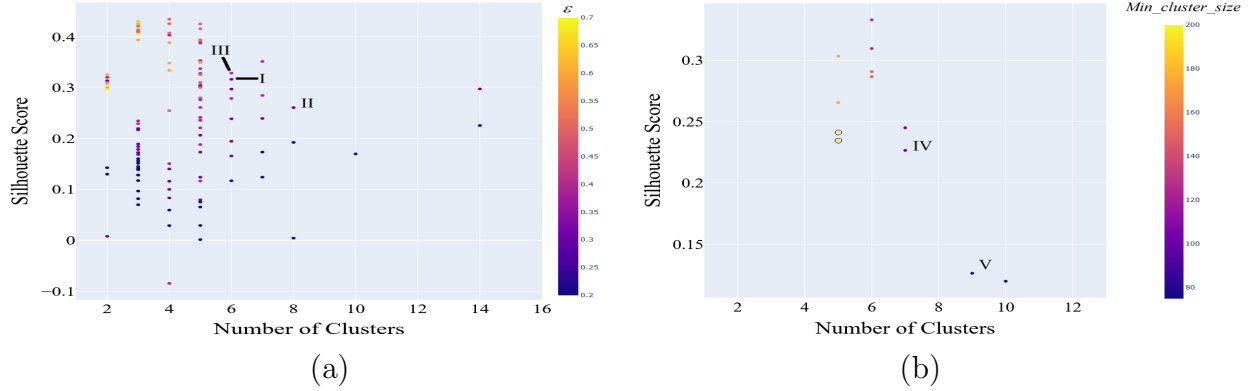


Figure 1: Silhouette index vs number of clusters evaluated for DBSCAN (a) and for HDBSCAN (b). Roman numerals I – V stand for the cases considered in the studies.

can be observed, when we consider the case I at $\varepsilon = 0.3$, $Min_samples = 100$, and metric = "euclidean"; case II at $\varepsilon = 0.3$, $Min_samples = 75$, and metric = "manhattan" (Fig. 1a). The values of Silhouette indices for specified clusters are listed in Table 1, where the numbers correspond to the cluster numbers including (–1) standing for outliers (noise points). All clusters possess acceptable Silhouette indices. The locations of clusters corresponding to the case I are illustrated in Fig. 2a, while those for case II are shown in Fig. 2b.

Although we eliminate the set of outliers from the further consideration, as was done in many studies [17, 18, 23, 30], it is still worth noting that they may hold potential interest for research. Furthermore, these outliers could correspond to background seismicity, as discussed by [24, 25].

For a more reasonable choice, we offer a division into clusters to compare with the fault network in the Caucasus region [2, 42, 43]. This approach is also used by [16, 21]. A comparison of the clustering identified using the Silhouette index with faults is drawn in Fig. 2 and testifies their excellent correlation. In other words, the densest accumulations of earthquakes are identified as clusters, and the location of the clusters correlates quite well with the compaction and intersection of major faults.

Remark:

1. Case III represents the partition into 6 clusters with the higher Silhouette index ($\varepsilon = 0.4$, $Min_samples = 125$, and metric = "manhattan"). This partition differs from the case I, however, as the data in Table 1 indicate, this difference is insignificant, at least in terms of Silhouette coefficients. Formally, to obtain the partition of the case III, we should consider the case I, shown in Fig. 2a, split Cluster 3 into two clusters, and eliminate Cluster 6, remaining other clusters unchanged, with the possible exception of a few points. Comparing these two partitions, I and III, with the fault network led us to prefer the partition I (Fig. 2a).
2. In addition to the Silhouette index, we also calculated CH and DB indices. Interestingly, CH indices for the cases I and II reach their maxima among the partitions consisting of 6 and 8 clusters, respectively. This means that corresponding clusters are dense and well separated. DB indices for the cases I and II do not reach minimum values, although they do not differ significantly from them.

Table 1: Silhouette index for the clusters obtained by DBSCAN algorithm and shown in Fig.2

	outliers	1	2	3	4	5	6	7	8	$Slh(C)$
case I	−0.523	0.400	0.594	0.642	0.767	0.648	0.699	–	–	0.316
case II	−0.568	0.469	0.608	0.677	0.729	0.653	0.743	0.833	0.655	0.261
case III	−0.507	0.748	0.622	0.648	0.702	0.649	0.802	–	–	0.323

2.3 Clustering of Earthquake Catalog using HDBSCAN algorithm

Now we apply the HDBSCAN algorithm, an advanced version of the DBSCAN, which constructs a hierarchical density-based cluster tree. This approach enables more robust and stable identification of clusters, particularly in datasets with varying densities such as earthquake catalogs. Unlike DBSCAN, HDBSCAN does not require the ε parameter. Instead, it uses other hyperparameters, such as *Min_cluster_size* and a distance metric, as described by [33]. Other HDBSCAN parameters are used by default according to the HDBSCAN class description provided by [41].

As in the preceding section, we use a similar technique for choosing the parameter *Min_cluster_size*, to identify the partitions consisting of at least six clusters. Thus, we specify the range $Min_cluster_size \in [75; 200]$ with an increment of 25. The metric used coincides with “*euclidean*” or “*manhattan*”.

The results of the clustering procedure are summarized in Fig. 1b, which shows the relationship between the Silhouette score and the number of clusters obtained for each parameter combination.

Analyzing Fig. 1b, we can see pairs of points. These pairs correspond to the partitions with different metrics. It turned out that they differ insignificantly. As shown in Fig. 1b, an increase in *Min_cluster_size* leads to a decrease in the number of clusters, and a reduction in *Min_cluster_size* leads to an increase.

Table 2: Silhouette index for the clusters obtained by HDBSCAN algorithm and shown in Fig. 3.

	outliers	1	2	3	4	5	6	7	8	9	$Slh(C)$
case IV	−0.584	0.741	0.724	0.819	0.745	0.667	0.808	0.734	–	–	0.226
case V	−0.633	0.769	0.743	0.602	0.821	0.793	0.533	0.696	0.802	0.732	0.126

Comparison with the fault network in combination with taking into account the high Silhouette index shows that the optimal options for partitions can be sets of 7 and 9 clusters. The case IV is observed at $Min_cluster_size = 100$, the case V is implemented at $Min_cluster_size = 75$. For both cases, metric = “*manhattan*”. The Silhouette indices for selected partitions are shown in Table 2, where, as above, the numbers from 1 to 9 mark the cluster numbers, (−1) relates to outliers, $Slh(C)$ marks the Silhouette index for the entire dataset. The data analysis shows that the positive $Slh(C)$ is 0.6 for Fig. 3a and 0.5 for Fig. 3b, which indicates a good quality of partitioning. *CH* and *DB* indices showed trends rather similar to the Silhouette score. In particular, the case IV has a *CH* value close to the maximum, while its *DB* index reaches a minimum among 7-cluster partitions. The

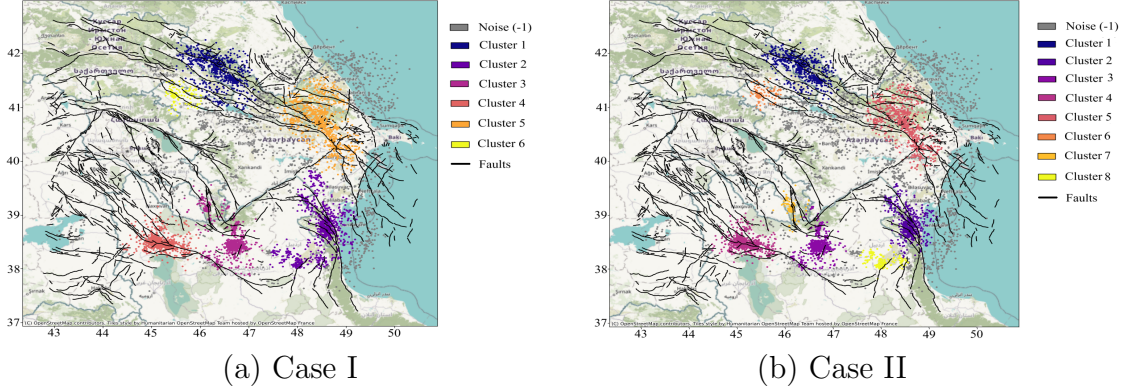


Figure 2: The earthquake clustering by DBSCAN algorithm. The following groups are marked: outliers (item Noise (-1) in the legends) and 6 clusters (a) and 8 clusters (b). The fault network is depicted by solid curves.

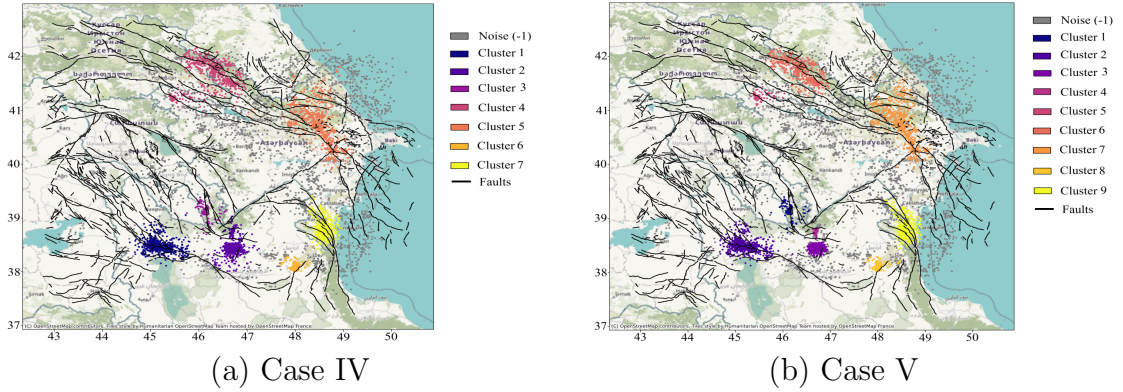


Figure 3: The earthquake clustering by HDBSCAN algorithm. The following groups are marked: 7 clusters (a), 9 clusters (b), and the sets of outliers. The fault network is depicted by solid curves.

location of selected partitions corresponding to the cases IV and V is shown in Fig. 3a and b, respectively.

3 Construction of the distance distributions for clusters

Constructing the partition among clusters, we identified seismically active zones, which, from the information point of view, are the most significant datasets and contain the most common features. It is further natural to investigate the statistical properties of clusters and the connection of these formations with selected points representing, for instance, strategically essential objects such as the Shamkir HPS. This station is part of a whole conglomerate of objects in this region, including large Mingachevir, Yenikend, and Shamkir water reservoirs and power stations providing the lion's share of the power supply to Azerbaijan. This explains this region's extensive geological and geophysical studies [6, 44].

This research studies the distribution of the random variable, which is the distance from an arbitrary fixed point to cluster points. Note that in the paper of [45] the advantages of

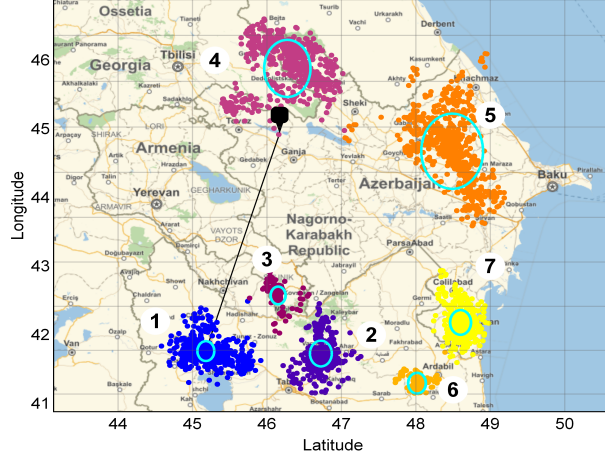


Figure 4: The location of the clusters (the numbers 1–7) from Fig. 3a with dropped outliers. Geomarker corresponds to the Shamkir HPS. The circles bound the domains, for which the CDFs and PDFs are constructed in Sec. 3.2.

such a study method have been emphasized, including independence on system coordinates and grid selection. It should also account for the significant achievements in probability theory and its application in geometry [46, 47].

Thus, let us consider the specified cluster C as a set of random points, defining random vectors from the fixed point $A(a, b)$ to a point $X(x, y)$ representing an epicenter of a random earthquake from cluster C . Let the random quantity W be the norm of the random vector

$$W = \|A - X\| = \sqrt{(x - a)^2 + (y - b)^2}. \quad (2)$$

We will further call the vector norm (2) the distance between points, although it is proportional to the traditional distance on the terrain, measured in length units. It is worth noting that it is impossible to carry out comprehensive theoretical studies of this issue in a general formulation due to the limitation of theoretical means. Instead, one can make progress in solving this problem by accepting some auxiliary hypotheses.

3.1 Distribution of distances from the cluster center to cluster random points

Now, we are going to construct the distance distribution when a fixed point coincides with the cluster center located at the point with coordinates $Q(m_X, m_Y)$, where m_X and m_Y are mean values of the coordinates of the cluster point.

Let us recall the classical result: if the coordinates of cluster points are independent and normally distributed $N(0, \sigma)$, then the distance (2) has the Rayleigh distribution with the parameter σ . Therefore, comparing empirical and Rayleigh distributions for the cluster allows one to estimate the correctness of assumptions regarding the distribution of cluster points.

Next, the corresponding CDF for the random variable W reads as follows

$$F(z) = P(W < z). \quad (3)$$

Analytical studies of the function $F(z)$ can be performed in a few cases. In particular, the analytical expression for $F(z)$ can be derived, as shown in Appendix A, when the coordinates of epicenters of earthquakes are jointly normally distributed and the point of consideration is the cluster center. Such assumptions are quite frequently used in statistical seismology, for instance, during the construction of scattering ellipses for clusters [16], Gaussian-mixture model construction [48].

In what follows the corresponding CDF for the random variable W reads as follows for the correlated normally distributed variables X and Y , we obtain

$$F(z) = \frac{1}{\sigma_X \sigma_Y \sqrt{2H}} \int_0^{z^2} \exp\left(-\frac{u(\sigma_x^{-2} + \sigma_y^{-2})}{H}\right) I_0(u \cdot \Delta) du, \quad (4)$$

where $H = 2(1 - r^2)$ (other designations see in Appendix A). By definition, PDF is also described by the following expression

$$PDF(z) = \frac{dF(z)}{dz}, \quad (5)$$

which defines the Rayleigh-like distribution.

Let us consider the functions (5) for each cluster of earthquakes under the above assumptions. Figure 5 shows the histograms for the variable W defined by (2). Dashed curves depict the approximations of the histograms by functions (5).

We also succeeded in approximating the histograms directly using numerical methods. Specifically, we apply the approach based on the PDF approximation by the Johnson curves [49, 50]. Step-by-step implementation of the algorithm described in Appendix B in detail allows one to get pretty good agreement between the approximating curve and the histogram, as seen from the analysis of Fig.5, where solid lines indicate the Johnson curves.

Note that all approximations fit well with the histograms, except for clusters 3 and 5, whose histograms differ significantly from Rayleigh-like profiles. One possible reason for the discrepancy between the histogram and the theoretical PDF can be a violation of the conditions for obtaining expression (5). In particular, the small number of points in cluster 3 may not be sufficient to confidently determine the statistical distribution. Another contributing factor could be a significant deviation of the distribution of points in the cluster from normal. Consequently, as in cases of the histograms for clusters 3 and 5, non-Rayleigh distributions for distances emerge. Such distributions can be better approximated by bimodal distributions, representing a mixture of two unimodal Rayleigh or normal distributions. A more detailed consideration of this issue requires auxiliary studies.

3.2 Distribution of distances from the fixed point lying beyond the cluster to cluster random points

Now, we consider the case when the fixed point $A(a, b)$ lies outside the cluster. Without restriction of generality, assume that it coincides with the coordinates of the Shamkir HPS $(a, b) = (40.93, 46.17)$. Its location is depicted in Fig.4 by the corresponding geomarker. Let us construct the distribution functions for the random variable W , which is a distance from the fixed point A to points of each cluster from Fig.4.

To conduct theoretical explorations, we should make certain additional assumptions. In particular, we assume that the cluster lies in a closed region. In the simplest case, we consider

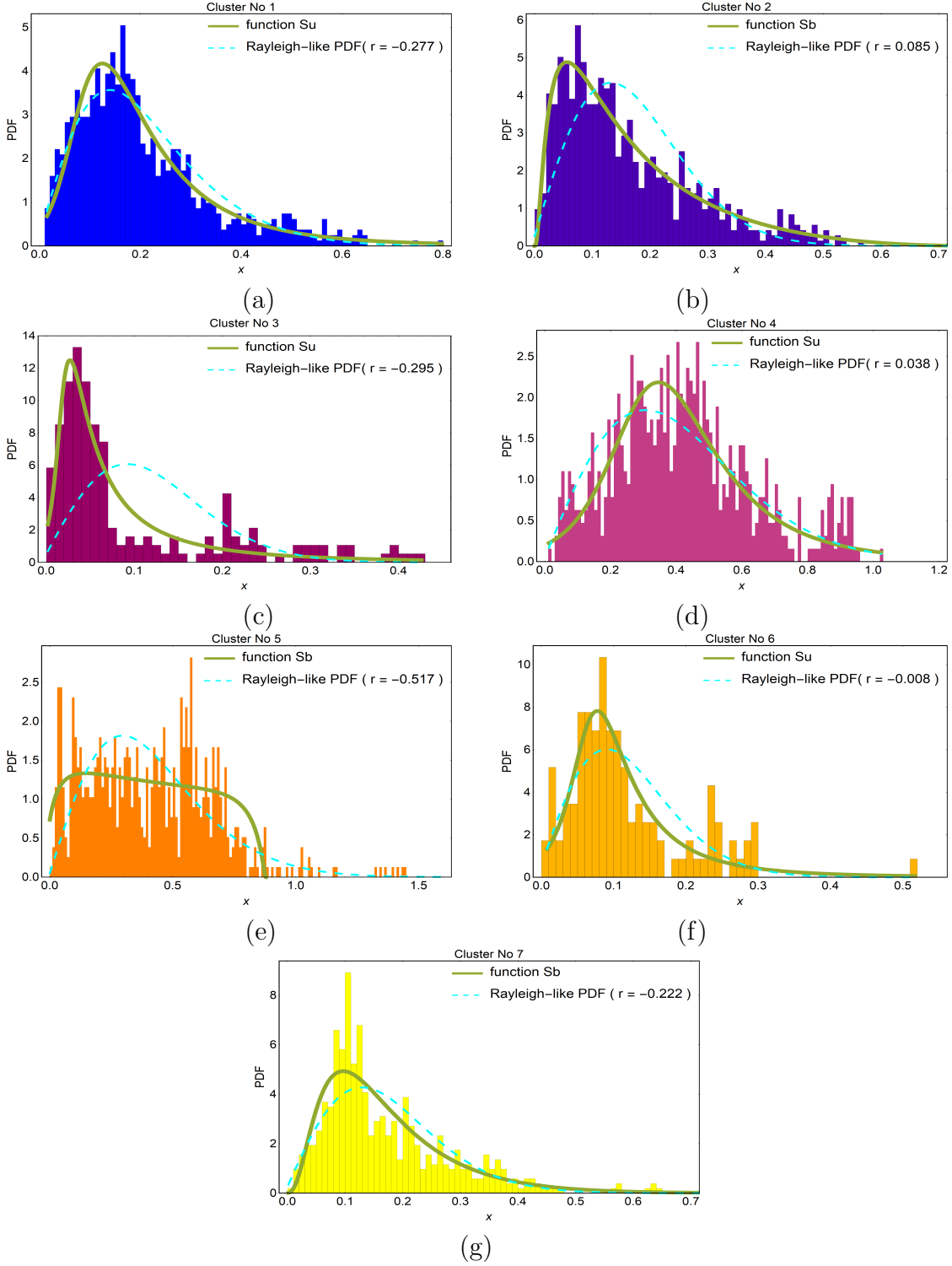


Figure 5: The approximation of histograms for the distances from the cluster center to its points. The cluster locations are shown in Fig.4 (the colors of clusters and histograms are the same). Dashed lines mark the Rayleigh-like distributions defined by (5), while solid lines depict the Johnson curves.

it to be a circle in which the points are uniformly distributed. This leads us to the classical problem, which admits an analytical solution [47], p.187.

In particular,

$$CDF(z) = \begin{cases} 0, & \text{if } z \leq R - q, \\ \frac{1}{\pi q^2} (q^2 \{\psi - \frac{1}{2} \sin 2\psi\} + z^2 \{\phi - \frac{1}{2} \sin 2\phi\}), & \text{if } R - q < z \leq R + q, \\ 1. & \text{otherwise,} \end{cases} \quad (6)$$

and

$$PDF(z) = \begin{cases} \frac{2z\phi}{\pi q^2}, & \text{if } R - q \leq z \leq R + q, \\ 0, & \text{otherwise,} \end{cases} \quad (7)$$

where

$$\cos \psi = (-z^2 + R^2 + q^2)/(2zR), \quad \cos \phi = (z^2 + R^2 - q^2)/(2zR), \\ R = \sqrt{(m_X - a)^2 + (m_Y - b)^2}$$

is the distance from Shamkir HPS to the cluster center and q is the circle radius.

So, let's place the circle center in the cluster's center and choose the circle radius proportional to the standard deviation $\min\{\sigma_X, \sigma_Y\}$. The circle center can be placed at another point, for instance, in (Moda X; Moda Y). The radius should be small so that the hypothesis of a uniform distribution would be more plausible. Fig. 6 shows a comparison of histograms and corresponding curves at different radii values of circles containing cluster points. An idea of the approximation of clusters by the specified circles can be obtained from the map in Fig. 4. When constructing the circles, smaller values of r_D were chosen from Fig. 6, i.e., for cluster 1, we take $r_D = 1.0 \min\{\sigma_X, \sigma_Y\}$ etc.

Utilizing the constructed functions (7) and (6), one can estimate the probability of the event B – the distance from the Shamkir HPS to an earthquake of the specified cluster lies in the interval $R - q < W < R - (2/3)q$. Using the definition of geometric probability, it is easy to understand that the region corresponding to the event B is the lens-shaped domain formed by the intersection of two radii, $R - q$ and $R - (2/3)q$ disks. This domain may be called the near zone of the cluster relative to the fixed external point A , which is the Shamkir HPS. Then, we obtain

$$P(B) = \int_{R-q}^{R-(2/3)q} PDF(z) dz = CDF(R - (2/3)q).$$

For the clusters from Fig. 4, the values of these probabilities are shown in Table 3. It follows

Table 3: The values of $P(B)$ for 7 clusters

No. of clrs.	1	2	3	4	5	6	7
$P_i(B)$	0.10726	0.10697	0.10660	0.08885	0.10211	0.10830	0.10762

from the analysis of Table 3 that the largest values of $P(B)$ correspond to clusters 1, 2, 3, 6, and 7, located at a greater distance from Shamkir HPS than clusters 4 and 5. This means that the probability of earthquake occurrence in the near zone is higher for the former

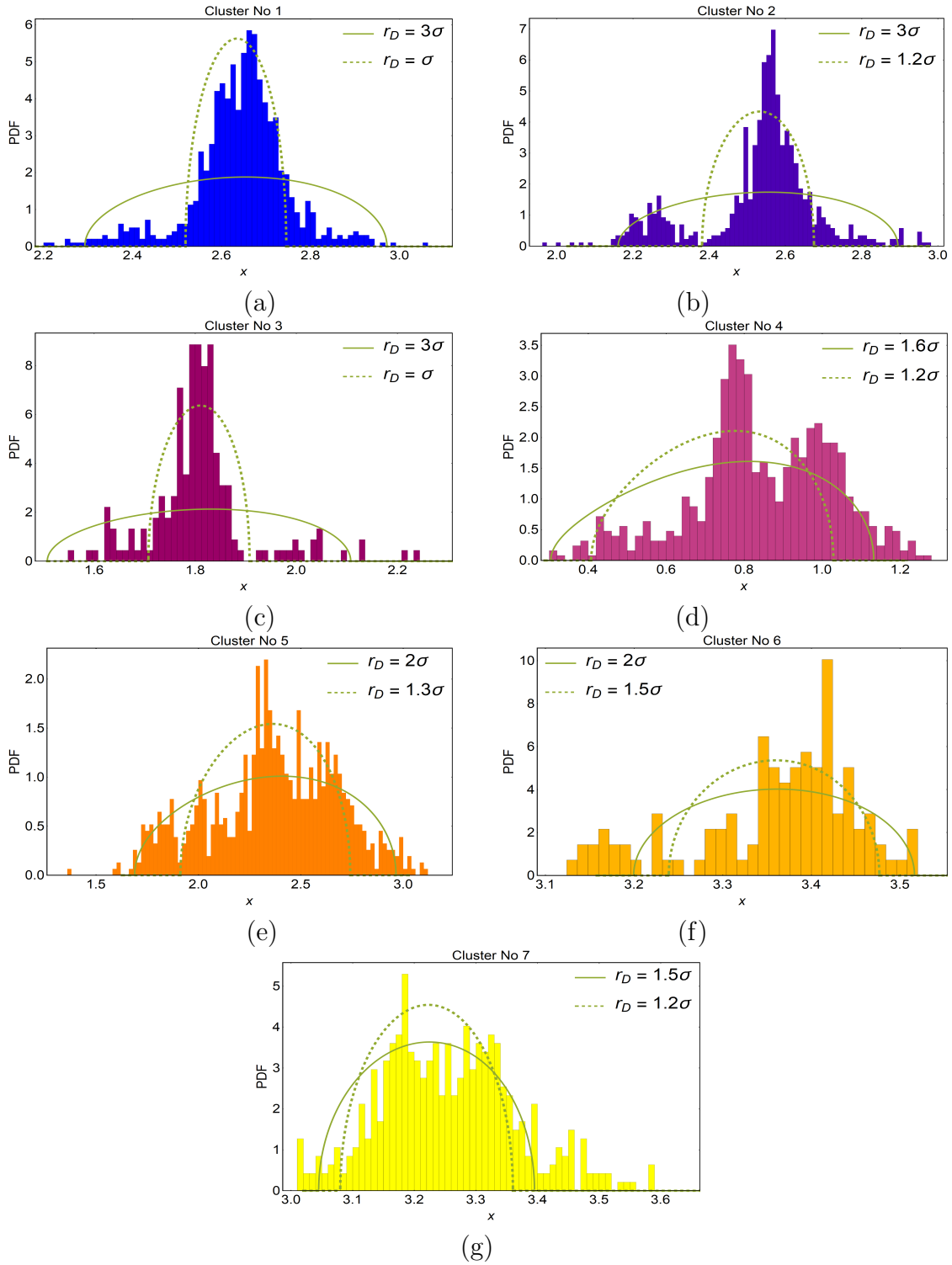


Figure 6: The approximations of histograms of distances from the Shamkir HPS to points of clusters depicted in Fig.4.

clusters than that of the latter cluster group. This may be related to the higher density of cluster regions bounded by circles and incorporated in studies.

Though the obtained findings concern the simplified problem, this problem can help assess the seismic risks of objects, classify territories, and improve insurance compensation algorithms.

4 Conclusions

Thus, the studies presented above are concerned with the seismicity of Azerbaijani territories, with a particular focus on the peculiarities of the spatial distribution of earthquake epicenters. Since the region's seismicity is inherently heterogeneous, analyzing the entire earthquake dataset is not always efficient. This encourages the selection of zones that are more prone to earthquakes and are more seismogenic. Cluster analysis proves helpful in this regard. It is worth noting that cluster analysis operates with numerical data; therefore, the results of its application are not unique and require additional information for decision-making.

Using the DBSCAN and HDBSCAN clustering algorithms, the earthquake catalog was partitioned into clusters. The number of clusters was validated through Silhouette index evaluation and its alignment with the fault network. The derived partitions generally resemble each other, accurately mapping the primary areas of dense epicenter concentration.

Subsequently, the partition consisting of 7 clusters was selected, and its statistical properties were analyzed. Specifically, cumulative and density probability functions were constructed for the random variable representing the distance from a fixed point on the ground surface to the epicenters comprising the clusters in the selected partition. Generally, this problem lacks analytical solutions; however, it can be addressed in two specific cases.

When the fixed point coincides with the cluster center and the epicenters distribution is binormal, the cumulative function can be presented via the integral relation, which effectively approximates the histogram of random distances. In this case, the Johnson curves, which are modifications of Gaussian curves, are evaluated numerically for the histograms. A comparison of theoretical and numerical approximants showed good agreement with the results. Analytical studies are also applicable when the fixed point lies outside the clusters. In this case, we used the solution of the classical problem.

The resulting cumulative distribution function approximates the histograms of distances from the fixed point, representing the location of the Shamkir HPS, to the epicenters. This assumes their uniform distribution over the clusters, whose boundaries were approximated by circles. Although this is a rather rough approximation, the comparison between theoretical PDFs and histograms shows good agreement in the results.

Using the constructed PDFs, the probability of the nearest earthquakes from the selected cluster relative to the Shamkir HPS was evaluated. These findings can help assess the seismic risk for the Shamkir HPS and other strategic objects, including the Mingachevir HPS.

Data availability

The earthquake catalog used in the current study is available at <http://www.isc.ac.uk/iscbulletin/search/>. The fault catalog is available at http://neotec.ginras.ru/index/english/database_eng.html. Python source code implementing the cluster analysis of the earthquake catalog is available at <https://github.com/SkurativskaKateryna/>

Appendices

A Calculation of the distribution function for W

To construct the CDF for the random variable W , we assume that random points in a cluster are distributed by the bivariate normal distribution

$$f_{XY} = \frac{1}{2\pi\sigma_X\sigma_Y\sqrt{1-r^2}} \exp\left(-\frac{1}{2(1-r^2)} \left[\frac{(x-m_X)^2}{\sigma_X^2} - \frac{2r(x-m_X)(y-m_Y)}{\sigma_X\sigma_Y} + \frac{(y-m_Y)^2}{\sigma_Y^2} \right]\right)$$

with the correlation coefficient r and the scattering center (m_X, m_Y) . Then, by definition, the CDF for W reads as follows:

$$F(z) = P(W < z) = \iint_G f_{XY} dx dy, \quad (8)$$

where $G : (x-a)^2 + (y-b)^2 < z^2$.

Transitioning from cartesian coordinates (x, y) to the polar coordinates (ρ, θ) by means of the well-known relations $x = m_X + \rho \cos \theta$, $y = m_Y + \rho \sin \theta$, one obtains

$$F(z) = \frac{1}{2\pi\sigma_X\sigma_Y\sqrt{2H}} \int_0^{z^2} e^{-u(\sigma_X^2+\sigma_Y^2)/(2H)} du \int_0^{2\pi} \exp\left(\frac{u(\sigma_Y^2-\sigma_X^2)}{2H} \cos 2\theta - \frac{u \cdot r}{2H\sigma_X\sigma_Y} \sin 2\theta\right) d\theta,$$

where $H = 2(1-r^2)$.

The integral over θ can be written in the following form

$$\int_0^{2\pi} \exp[u\Delta \cos(2\theta + \theta_0)] d\theta,$$

where $\Delta = \sqrt{\left(\frac{\sigma_Y^2-\sigma_X^2}{2H}\right)^2 + \left(\frac{r}{2H\sigma_X\sigma_Y}\right)^2}$ and $\theta_0 = \arctan \frac{r}{\sigma_X\sigma_Y(\sigma_Y^2-\sigma_X^2)}$.

The next change of variable $2\theta + \theta_0 = \eta$ leads this integral to the expression

$$\frac{1}{2} \int_{\theta_0}^{4\pi+\theta_0} \exp[u\Delta \cos \eta] d\eta.$$

Taking into account the well-known property of integration of T -periodic function, i.e. $\int_a^{T+a} f(t)dt = \int_0^T f(t)dt$, we arrive to the ultimate result

$$\frac{1}{2} \int_0^{4\pi} \exp[u\Delta \cos \eta] d\eta = 2\pi I_0(u\Delta).$$

It turned out that the derived integral can be written via the modified Bessel function of the first kind

$$I_0(x) = \pi^{-1} \int_0^\pi \exp(x \cos \theta) d\theta, \quad I_0(0) = 1.$$

It is easy to prove that $\int_0^{n\pi} \exp(x \cos \theta) d\theta = \pi n I_0$. This transcendental function as a rule is defined in many packages for technical computing including *Mathematica*, where the function `BesselI[0, x]` is introduced.

Thus, performing the transformations outlined above, we can present the function $F(z)$ in the form of the expression (4).

As it follows from (4), when the coordinates of a random point are *independent* and distributed normally by $N(0, \sigma)$, i.e. $\sigma_X = \sigma_Y = \sigma$ and $r = 0$, then W is distributed by Rayleigh distribution with PDF

$$f(z) = \frac{dF}{dz} = \frac{z}{\sigma^2} \exp\left(-\frac{z^2}{2\sigma^2}\right). \quad (9)$$

Let us also note that at small r the function $f(z)$ is close to the Rayleigh distribution.

B Construction of the Johnson curves for the random variable W

The algorithm is realized by the tools of the package “Mathematica”. Let us describe the main stages for the construction of Johnson curves.

First, we should form the dataset of the quantity W and sort it in ascending order. We also fix, as it has done in the papers [49, 50], the value $z = 0.524$ and evaluate probabilities

$$P_z = \text{CDF}[\text{NormalDistribution}[0, 1], z] = 0.699861,$$

$$P_{3z} = \text{CDF}[\text{NormalDistribution}[0, 1], 3z] = 0.942025,$$

$$P_{-z} = \text{CDF}[\text{NormalDistribution}[0, 1], -z] = 0.300139,$$

$$P_{-3z} = \text{CDF}[\text{NormalDistribution}[0, 1], -3z] = 0.0579753,$$

using the in-built cumulative distribution function `CDF[.]` for the normal distribution $N(0, 1)$.

Next, we calculate discriminant

$$\Delta = \frac{mn}{p^2}.$$

For 7 clusters from Fig.4, we have $\Delta = \{1.28196, 0.713116, 1.4699, 1.62483, 0.394042, 1.9467, 0.89797\}$. Since $\Delta_{1,3,4,6} > 1$, we should choose the Johnson S_u curve, while for $\Delta_{2,5,7} < 1$ the curve S_b should be chosen. These functions (Mathematica syntax) are defined as follows

$$S_u(z) = \frac{\eta\lambda}{\sqrt{1 + \frac{(z-\epsilon)^2}{\lambda^2}}} \text{PDF} \left[\text{NormalDistribution}[0, 1], \gamma + \eta \text{ArcSinh} \frac{z - \epsilon}{\lambda} \right] \quad (10)$$

and

$$S_b(z) = \frac{\eta\lambda}{(z - \epsilon)(\lambda + \epsilon - z)} \text{PDF} \left[\text{NormalDistribution}[0, 1], \gamma + \eta \log \left[\frac{z - \epsilon}{\lambda + \epsilon - z} \right] \right]. \quad (11)$$

The proper parameter values of each function can be found in [49, 50].

Remark: Roughly speaking, the quantity Δ_6 can be considered as close to 1, and then, instead of S_b , one can use the function $S_l(z)$ defined by the expression

$$S_l(z) = \frac{\eta}{z - \epsilon} \text{PDF} [\text{NormalDistribution}[0, 1], \gamma + \eta \log [z - \epsilon]].$$

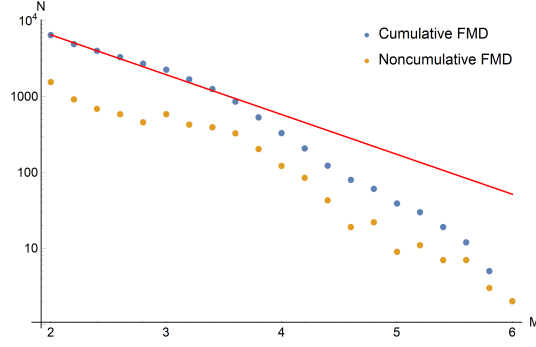


Figure 7: Estimation of the completeness magnitude M_c using the MAXC method [5].

It is obvious that S_l is simpler than S_b . The profiles of these functions differ insignificantly and approach each other when Δ tends 1. In this research, we used the functions S_b and S_u only.

C Evaluation of the completeness magnitude M_c

To evaluate the completeness magnitude M_c , we consider the cumulative and non-cumulative frequency-magnitude distributions (FMDs) and use the MAXC method [5, 12, 24]. The results of calculations are shown in Fig.7, where $M_c = 2$ corresponds to the magnitude for the highest frequency in the noncumulative FMD. The GR law $\log_{10}N = a - bM$ with $a = 4.86$ and $b = 0.52$ (solid straight line in Fig.7) was also evaluated. Note that similar but more comprehensive evaluations of M_c for Azerbaijan earthquakes that occurred from 2003 to 2016 were performed by [5], where, in particular, $M_c = 2.1$ was determined using the MAXC method (see Fig.5a in [5]) and corresponding parameters for the GR law $a = 4.45$ and $b = 0.507$ were calculated. These values are close to our results. Finally, taking into account the fact that M_c usually decreases with time in most catalogs [12] and exhibits significant spatial heterogeneity, varying by an order of magnitude [12], we can conclude that the completeness magnitude $M_c = 2$ for our studies is quite appropriate estimate for the lower magnitude threshold of the earthquake catalog used in our study.

D The parameter estimation for DBSCAN

To select the parameter ε and $Min_samples$ for the DBSCAN algorithm, let us consider the sorted k -distance graph mentioned in the papers [19, 31], using the sorted distance matrix. We start from plotting the 4-distance graph (Fig. 8), where the ε value relates to the “knee” formation on the graph. Analysis of k -distance graphs obtained at $k = 100$ and $k = 350$ shows that the corresponding “knee” value of ε increases, as k increases. However, as noted in [11, 20], this procedure should still be considered as an approximate method for parameter estimation.

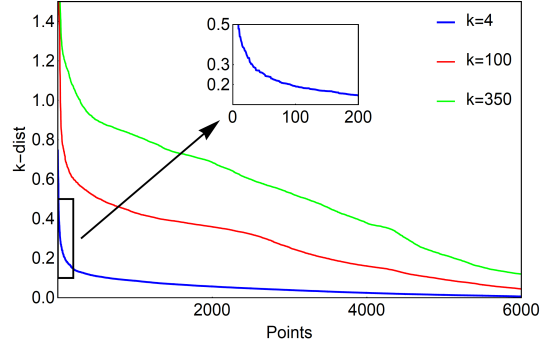


Figure 8: The sorted k -distance graphs.

References

- [1] GeoNet, “Earthquake statistics,” 2024, figshare <https://www.geonet.org.nz/earthquake/statistics>.
- [2] N. Tsereteli, A. Tibaldi, V. Alania, A. Gventsadse, O. Enukidze, O. Varazanashvili, and B. Müller, “Active tectonics of central-western Caucasus, Georgia,” *Tectonophysics*, vol. 691, pp. 328–344, 2016, DOI: <https://doi.org/10.1016/j.tecto.2016.10.025>.
- [3] M. Bochud, “Tectonics of the Eastern Greater Caucasus in Azerbaijan,” Doctoral thesis, University of Fribourg (Switzerland), 2011, <https://folia.unifr.ch/unifr/documents/302897>.
- [4] T. Kangarli, T. Mammadli, F. Aliyev, R. Safarov, and S. Kazimova, “Revelation of potentially seismic dangerous tectonic structures in a view of modern geodynamics of the Eastern Caucasus (Azerbaijan),” in *Earth’s Crust and Its Evolution*, M. Cengiz and S. Karabulut, Eds. Rijeka: IntechOpen, 2021, ch. 9, DOI: 10.5772/intechopen.101274.
- [5] L. Telesca, F. Kadirov, G. Yetirmishli, R. Safarov, G. Babayev, and S. Ismaylova, “Statistical analysis of the 2003–2016 seismicity of Azerbaijan and surrounding areas,” *Journal of Seismology*, vol. 21, no. 6, p. 1467–1485, 2017, DOI: <https://doi.org/10.1007/s10950-017-9677-x>.
- [6] A. Tibaldi, F. L. Bonali, F. Pasquaré Mariotto, P. Oppizzi, N. Tsereteli, H. Havenith, G. Babayev, and T. Pánek, “Structural expression of the frontal thrust of an active fold-and-thrust belt: The Holocene 123-km-long Kur fault, Greater Caucasus, Azerbaijan,” *Journal of Structural Geology*, vol. 180, p. 105085, 2024, DOI: <https://doi.org/10.1016/j.jsg.2024.105085>.
- [7] T. Tjong-Kie, Z. Jian-Zhong, L. Jin, and Z. Ying, “Seismic patterns in Northern China and the characteristics of the epicentral distribution of the medium strong earthquakes before the large events,” *Tectonophysics*, vol. 138, no. 1, pp. 45–53, 1987, DOI: [https://doi.org/10.1016/0040-1951\(87\)90064-3](https://doi.org/10.1016/0040-1951(87)90064-3).
- [8] G. Ouillon and D. Sornette, “Segmentation of fault networks determined from spatial clustering of earthquakes,” *Journal of Geophysical Research: Solid Earth*, vol. 116, no. B2, p. B02306, 2011, DOI: <https://doi.org/10.1029/2010JB007752>.

- [9] Y. Semenova, O. Kendzera, S. Skurativskyi, S. Mykulyak, I. Skurativska, and O. Topoliuk, “Mitigating earthquake risks in the Shamkir-Mingachevir reservoir region through comprehensive ground response analysis,” 2024, paper presented at the 5th International Conference on Sustainable Futures: Environmental, Technological, Social and Economic Matters (ICSF 2024), Kryvyi Rih, Ukraine, May 2024. [Online]. Available: <https://icsf.easyscience.education/2024/index5.html>
- [10] O. Kendzera, Y. Semenova, O. Topoliuk, S. Skurativskyi, S. Mykulyak, I. Skurativska, O. Trypilska, and V. Drukarenko, “Seismic hazard evaluation and soil response analysis of Shamkir and Mingachevir hydroelectric power stations,” 2024, paper presented at the EGU General Assembly Conference, Wien, April 2024. DOI: 10.5194/egusphere-egu24-11911.
- [11] S. Cesca, “Seiscloud, a tool for density-based seismicity clustering and visualization,” *J. Seismol.*, vol. 24, p. 443–457, 2020, DOI: 10.1007/s10950-020-09921-8.
- [12] S. Wiemer and M. Wyss, “Minimum magnitude of completeness in earthquake catalogs: examples from Alaska, the western United States, and Japan,” *Bulletin of the Seismological Society of America*, vol. 90, no. 4, p. 859–869, 2000, DOI: <https://doi.org/10.1785/0119990114>.
- [13] ISC, “International seismological centre (2024). on-line bulletin,” 2024, figshare <http://www.isc.ac.uk/iscbulletin/search/>.
- [14] O. Nicolis, L. Delgado, B. Peralta, M. Díaz, and M. Chiodi, “Space-time clustering of seismic events in Chile using ST-DBSCAN-EV algorithm,” *Environ Ecol Stat*, vol. 31, p. 509–536, 2024, DOI: <https://doi.org/10.1007/s10651-023-00594-3>.
- [15] C. Hennig, M. Meila, F. Murtagh, and R. Rocci, Eds., *Handbook of Cluster Analysis*. New York: CRC Press, 2016.
- [16] A. Ansari, A. Noorzad, and H. Zafarani, “Clustering analysis of the seismic catalog of Iran,” *Computers & Geosciences*, vol. 35, p. 475–486, 2009, DOI: <https://doi.org/10.1016/j.cageo.2008.01.010>.
- [17] S. Cesca, A. T. Şen, and T. Dahm, “Seismicity monitoring by cluster analysis of moment tensors,” *Geophys. J. Int.*, vol. 196, no. 3, pp. 1813–1826, 2013, DOI: 10.1093/gji/ggt492.
- [18] W. L. Yeck, L. V. Block, C. K. Wood, and V. M. King, “Maximum magnitude estimations of induced earthquakes at Paradox Valley, Colorado, from cumulative injection volume and geometry of seismicity clusters,” *Geophys. J. Int.*, vol. 200, no. 1, pp. 322–336, 2014, DOI: 10.1093/gji/ggu394.
- [19] Z. Fan and X. Xu, “Application and visualization of typical clustering algorithms in seismic data analysis,” *Procedia Computer Science*, vol. 151, pp. 171–178, 2019, DOI: 10.1016/j.procs.2019.04.026.
- [20] E. Piegari, M. Herrmann, and W. Marzocchi, “3-D spatial cluster analysis of seismic sequences through density-based algorithms,” *Geophys. J. Int.*, vol. 230, no. 3, pp. 2073–2088, 2022, DOI: 10.1093/gji/ggac160.

- [21] M. Taroni, R. Consoler, C. Montuori, M. Murru, G. Falcone, L. Chiaraluce, and A. L. Pastoressa, “Statistically significant difference between earthquake size distributions of independent and triggered seismicity,” *Commun. Earth Environ.*, vol. 5, p. 193, 2024, DOI: <https://doi.org/10.1038/s43247-024-01367-x>.
- [22] R. K. Vijay and S. J. Nanda, “Seismicity analysis using space-time density peak clustering method,” *Pattern Anal. Applic.*, vol. 24, no. 9, p. 181–201, 2020, DOI: <https://doi.org/10.1007/s10044-020-00913-5>.
- [23] E. Sardeli, G. Michas, K. Pavlou, D. Zaccagnino, and F. Vallianatos, “Spatiotemporal properties of the 2020 – 2021 Petrinja (Croatia) earthquake sequence,” *J. Seismol.*, vol. 28, p. 899–920, 2024, DOI: [10.1007/s10950-024-10228-1](https://doi.org/10.1007/s10950-024-10228-1).
- [24] S. Mitchinson, J. H. Johnson, B. Milner, and J. Lines, “Identifying earthquake swarms at Mt. Ruapehu, New Zealand: a machine learning approach,” *Frontiers in Earth Science*, vol. 12, p. 1343874(21), 2024, DOI: [10.3389/feart.2024.1343874](https://doi.org/10.3389/feart.2024.1343874).
- [25] D. Essing and P. Poli, “Unraveling earthquake clusters composing the 2014 Alto Tiberina earthquake swarm via unsupervised learning,” *Journal of Geophysical Research: Solid Earth*, vol. 129, no. 1, p. e2022JB026237, 2024, DOI: <https://doi.org/10.1029/2022JB026237>.
- [26] I. Gonzalez Álvarez, M. Segou, and B. Baptie, “Tracing the central Italy 2016-2017 seismic sequence fault system: Insights from unsupervised machine learning and principal component analysis,” 2024, machine Learning in Geophysics UK Conference : University of East Anglia, Norwich, UK, 11-13 Sept 2023. [Online]. Available: <https://nora.nerc.ac.uk/id/eprint/535836>
- [27] S. Yano and S. Ide, “Event-feature-based clustering reveals continuous distribution of tectonic tremors of 0.3–100 s: Application to Western Japan,” *Geophysical Research Letters*, vol. 51, no. 19, p. e2024GL108874, 2024, DOI: <https://doi.org/10.1029/2024GL108874>.
- [28] M. Grunberg and S. Lambotte, “A new workflow for revising the seismicity catalog for mainland France, covering the period 2010-2018,” 2024, eGU General Assembly 2024, Vienna, Austria, 14–19 Apr 2024, EGU24-5100. [Online]. Available: <https://doi.org/10.5194/egusphere-egu24-5100>
- [29] E. Humphrey, “Spotting spatiotemporal patterns in earthquake data,” 2024, towards Data Science. [Online]. Available: <https://towardsdatascience.com/spotting-spatiotemporal-patterns-in-earthquake-data-b07068b84314/>
- [30] S. Scitovski, “A density-based clustering algorithm for earthquake zoning,” *Computers & Geosciences*, vol. 110, pp. 90–95, 2018, DOI: <https://doi.org/10.1016/j.cageo.2017.08.014>.
- [31] M. Ester, H.-P. Kriegel, J. Sander, and X. Xu, “A density-based algorithm for discovering clusters in large spatial databases with noise,” p. 226–231, 1996, proceedings of 2nd International Conference on Knowledge Discovery and Data Mining. [Online]. Available: <https://dl.acm.org/doi/10.5555/3001460.3001507>

- [32] R. Campello, D. Moulavi, and J. Sander, “Density-based clustering based on hierarchical density estimates,” in *Advances in Knowledge Discovery and Data Mining*, J. Pei, V. S. Tseng, L. Cao, H. Motoda, and G. Xu, Eds. Berlin, Heidelberg: Springer Berlin Heidelberg, 2013, pp. 160–172, DOI: https://doi.org/10.1007/978-3-642-37456-2_14.
- [33] L. McInnes, J. Healy, and S. Astels, “The hdbscan clustering library,” 2016, algorithm implementation in Python and related issues. [Online]. Available: <https://hdbscan.readthedocs.io/en/latest/>
- [34] O. Arbelaiz, I. Gurrutxaga, J. Muguerza, J. M. Pérez, and I. Perona, “An extensive comparative study of cluster validity indices,” *Pattern Recognition*, vol. 46, no. 1, pp. 243–256, 2013, DOI: <https://doi.org/10.1016/j.patcog.2012.07.021>.
- [35] R. Todeschini, D. Ballabio, V. Termopoli, and V. Consonni, “Extended multivariate comparison of 68 cluster validity indices. A review,” *Chemometrics and Intelligent Laboratory Systems*, vol. 251, p. 105117, 2024, DOI: <https://doi.org/10.1016/j.chemolab.2024.105117>.
- [36] Y. Liu, Z. Li, H. Xiong, X. Gao, and J. Wu, “Understanding of internal clustering validation measures,” in *2010 IEEE International Conference on Data Mining*, 2010, pp. 911–916, DOI: [10.1109/ICDM.2010.35](https://doi.org/10.1109/ICDM.2010.35).
- [37] P. J. Rousseeuw, “Silhouettes: A graphical aid to the interpretation and validation of cluster analysis,” *Journal of Computational and Applied Mathematics*, vol. 20, pp. 53–65, 1987, DOI: [https://doi.org/10.1016/0377-0427\(87\)90125-7](https://doi.org/10.1016/0377-0427(87)90125-7).
- [38] A. Dudek, “Silhouette index as clustering evaluation tool,” in *Classification and Data Analysis: Theory and Applications*, ser. Studies in Classification, Data Analysis, and Knowledge Organization, K. Jajuga, J. Batóg, and M. Walesiak, Eds. Cham: Springer International Publishing, 2020, pp. 19–33, DOI: https://doi.org/10.1007/978-3-030-52348-0_2.
- [39] X. He, *Cluster Analysis*. Singapore: Springer Nature Singapore, 2024, pp. 135–153, DOI: https://doi.org/10.1007/978-981-97-4022-2_7.
- [40] M. Ibrahim and B. Al-Bander, “An integrated approach for understanding global earthquake patterns and enhancing seismic risk assessment,” *International Journal of Information Technology*, vol. 16, no. 4, pp. 2001–2014, 2024, DOI: [10.1007/s41870-024-01778-1](https://doi.org/10.1007/s41870-024-01778-1).
- [41] F. Pedregosa, G. Varoquaux, A. Gramfort, V. Michel, B. Thirion, O. Grisel, M. Blondel, P. Prettenhofer, R. Weiss, V. Dubourg, J. Vanderplas, A. Passos, D. Cournapeau, M. Brucher, M. Perrot, and E. Duchesnay, “Scikit-learn: Machine learning in Python,” *Journal of Machine Learning Research*, vol. 12, pp. 2825–2830, 2011, on HDBSCAN class see <https://scikit-learn.org/stable/modules/generated/sklearn.cluster.HDBSCAN.html>.
- [42] E. Zelenin, D. Bachmanov, S. Garipova, V. Trifonov, and A. Kozhurin, “The Active Faults of Eurasia Database (AFEAD): the ontology and design behind the continental-scale dataset,” *Earth System Science Data*, vol. 14, no. 10, p. 4489–4503, 2022, DOI: <https://doi.org/10.5194/essd-14-4489-2022>.

- [43] A. Avagyan, M. Sosson, H. Philip, A. Karakhanian, Y. Rolland, R. Melkonyan, S. Rebaï, and V. Davtyan, “Neogene to Quaternary stress field evolution in Lesser Caucasus and adjacent regions using fault kinematics analysis and volcanic cluster data,” *Geodinamica Acta*, vol. 18, no. 6, pp. 401–416, 2005, DOI: 10.3166/ga.18.401-416.
- [44] T. H. Babayev, Y. N. Aliyev, I. B. Muradi, and M. M. Aliyev, “Seismic analysis of the Shamkir reservoir area through insights into the dynamics of the earthquake characteristics,” *ANAS Transactions, Earth Sciences*, vol. 2, pp. 51–63, 2023, DOI: 10.33677/ggianas20230200102.
- [45] Y. Y. Kagan, “Earthquake spatial distribution: the correlation dimension,” *Geophysical Journal International*, vol. 168, no. 3, p. 1175–1194, 2007, DOI: <https://doi.org/10.1111/j.1365-246X.2006.03251.x>.
- [46] M. G. Kendall and P. A. P. Moran, *Geometrical Probability*. London: Charles Griffin and Company Limited, 1963.
- [47] A. M. Mathai, *An Introduction to Geometrical Probability Distributional Aspects with Applications*, ser. Statistical distributions and models with applications. Vol.1. Amsterdam: Gordon and Breach Science Publishers, 1999.
- [48] F. Aden-Antoniów, W. B. Frank, and L. Seydoux, “An adaptable random forest model for the declustering of earthquake catalogs,” *Journal of Geophysical Research: Solid Earth*, vol. 127, p. e2021JB023254, 2022, DOI: <https://doi.org/10.1029/2021JB023254>.
- [49] N. R. Farnum, “Using Johnson curves to describe non-normal process data,” *Quality Engineering*, vol. 9, no. 2, pp. 329–336, 1996, DOI: <https://doi.org/10.1080/08982119608919049>.
- [50] J. F. Slifker and S. S. Shapiro, “The Johnson system: Selection and parameter estimation,” *Technometrics*, vol. 22, no. 2, pp. 239–246, 1980, DOI: <https://doi.org/10.1080/00401706.1980.10486139>.